

## Synergistic Effect of Barium Chloride on Corrosion Inhibition of Copper by Aqueous Extract of Lupine Seeds in Nitric Acid

Abd El-Aziz S. Fouda<sup>1, \*</sup>, Safaa El-din H. Etaiw<sup>2</sup>, Dina M. Abd El-Aziz<sup>2</sup>, and Osama A. Elbaz<sup>1</sup>

<sup>1</sup> Chemistry Department, Faculty of Science, Mansoura University, Mansoura-35516, Egypt

<sup>2</sup> Department of Chemistry, Faculty of Science, Tanta University, Tanta, Egypt

\*E-mail: [asfouda@hotmail.com](mailto:asfouda@hotmail.com)

Received: 7 December 2016 / Accepted: 23 April 2017 / Published: 12 June 2017

---

Synergistic effect of BaCl<sub>2</sub> on the corrosion inhibition efficiency of aqueous Lupine seed extract, on (Cu) in 2 M HNO<sub>3</sub> acid solution has been investigated using weight loss measurements, electrochemical impedance spectroscopy (EIS), electrochemical frequency modulation (EFM) and potentiodynamic polarization (PP) studies. The results show that inhibition efficiencies on Cu increase with increase in concentration of the extract and enhancement in inhibition efficiency was observed on addition of barium chloride due to synergism. The adsorptions, of extract and extract + BaCl<sub>2</sub> on the surfaces of the corroding metal obey Langmuir isotherms. Polarization studies revealed that lupine extract acts as a mixed type inhibitor. Thermodynamic parameters were calculated using the adsorption isotherms. A probable synergistic mechanism is proposed. The film coated on Cu specimens was analyzed by using Fourier transform infrared spectroscopy (FT-IR). The surface shape was studied by using atomic force microscopy (AFM) analysis.

---

**Keywords:** Corrosion inhibition, Lupine seed extract, HNO<sub>3</sub>, Cu, BaCl<sub>2</sub>, PP, EIS, EFM, AFM, FT-IR

### 1. INTRODUCTION

Copper and its alloys are widely used in the materials because of their excellent electrical and thermal conductivities in many applications such as electronics, [1] vacuum tubes, magnetrons in microwave oven and integrated circuits [2-4]. Copper is relatively noble metal, requiring strong oxidants for its dissolution or corrosion. The manufacturing of electronic devices is done by using the important processes like chemical dissolution and electrolytic plating. Nitric acid is most prevalent corrosive mediums, so this medium has induced a great deal of research on Cu corrosion [5-20]. Heat move is inversely proportional to the corrosion yield so increasing the corrosion product leads to the bad efficiency of the equipment. Periodic cleaning of the equipment and removing sediments is very

important so while the elimination of corrosion products the acid comes in contact with copper metal and corrosion happen [21]. Nitric acid is one of the more circle corrosive used on a large scale, so this medium is ideal to do research on copper corrosion [22]. The use of organic inhibitors is limited because of their environmental risk and ecological regulations. Plant extracts are readily available, safe, non-toxic, environmentally acceptable, ecofriendly and in addition to being a renewable source for a wide range of corrosion inhibitors. Green inhibitors are source of many low cost natural products. This natural product is safe on the environment and can be extracted by simple procedure [23]. Corrosion of the metal is prohibited by using these extracts. Lupine is a medicinal food plant with potential value in the management of diabetes [24]. Lupine extract was utilized in the corrosion prevention of zinc in 0.5 M alkaline medium [25], corrosion of 7075-T6 aluminum alloy in 0.5 M alkaline medium [26], corrosion of steel or iron in acid medium [27]. Corrosion of several metals and alloys was studied by using many plant extracts [28-47]. The plant extracts containing the bioactive compounds which are effective like synthetic inhibitors.

In this study, we focused on anti-corrosion performance of Lupine as an economical, environment friendly and the effectiveness of Lupine with  $\text{BaCl}_2$  for copper in 2 M  $\text{HNO}_3$  solution by WL, PP, EFM and EIS methods. The shape of the outer surface of the copper metal was studied by using FT-IR spectroscopy and AFM technique.

## 2. EXPERIMENTAL

### 2.1. Chemicals and materials

Electrochemical testing and surface scanning was tested on the commercial pure Cu which consists of (in weight %): 0.0050 Zn, 0.0023 Pb, 0.0023 P, 0.0018 Co, 0.0019 Al, 0.0015 Si, 0.004 Ni, 0.0011 S and rest Cu. Before every experiment copper must pass through several steps, step by step. Firstly, the surface is polished in the same direction using various emery papers to arrive the metal surface like mirror secondly the metal is washed with bidistilled water and finally it is dried at room temperature. Chemical reagent using in the experiments like ( $\text{HNO}_3$ ,  $\text{BaCl}_2$  and others) were obtained from Al-Gomhoria Company, Egypt. Prepare all working reagents using bidistilled water. Concentrated solution of lupine seeds extract was prepared by refluxing 10 g of dry coarsely powdered seeds in 100 mL of bidistilled water for one hour. The resulting solution was cleaned to remove any pollution. The concentration of the working solution was determined by evaporating 15 mL of the filtrate and weighing the residue. The concentrated working solution was diluted to several concentrations by bidistilled water in terms of g/l.

### 2.2. Preparation of Solutions

The destructive working solutions, 2M  $\text{HNO}_3$  were prepared by diluting of concentrated analytical grade (70%)  $\text{HNO}_3$  with bidistilled water. The concentrated solution of the lupine seed extract was diluted to 50-250 ppm by bidistilled water.

### 2.3. WL Method

Previously weight loss measurements were used in corrosion studies to determine the suitable inhibitor [48]. Different concentrations were prepared for testing corrosion on Cu metal for two hours. These concentrations consisted of 100 ml of blank without inhibitor and 2M HNO<sub>3</sub> with inhibitor. The WL values obtained after certain time is used in the mathematical equation (1) to calculate the %IE of the different solutions.

$$\%IE = \theta \times 100 = [1 - (W/W^{\circ})] \times 100 \quad (1)$$

Where W<sup>o</sup> is the value of the average weight loss of the blank (2M HNO<sub>3</sub>) alone and W is the value of the average weight loss of acid with addition of different concentrations of extract under study.

### 2.4. Electrochemical measurements

Electrochemical measurements were directed in a conventional three electrodes thermostated cell. The device used in the electrochemical tests coming from Gamry instruments company production. Reference 3000 is the model of this instrument. Electrolysis cell consists of Pyrex of cylinder closed by cap containing five openings. Three of them were used for the electrodes. The working electrode was Copper with the exterior area of 1x1 cm. Before each experiment, the electrode was refined using emery paper up to 1200 grades. After this, the electrode was cleaned ultra-sonically with purified water. Reference is a saturated calomel electrode (SCE). This electrode is reference to all presented potentials. The counter electrode consisted of platinum foil with an area of one centimeter square. Two molar HNO<sub>3</sub> solutions were used in this study as ideal corrosive media. All tests were carried out at temperature 25°C.

The software of Gamry instrument was adjusted to determine the Tafel polarization curves as follow. The electrode potential is automatically changed from - 280 to +200 mV<sub>SCE</sub> with a scan rate of 1 mV s<sup>-1</sup> after the steady state is reached (30 min) and the open circuit potential (OCP) was recorded. The corrosion current densities obtained from the Tafel plots were used in the mathematical equation (2) to calculate the IE.

$$\%IE = \theta \times 100 = [1 - (i_{\text{corr}}/i^{\circ}_{\text{corr}})] \times 100 \quad (2)$$

Where i<sup>o</sup><sub>corr</sub> is the corrosion current density of acid alone and i<sub>corr</sub> is the corrosion current densities of acid with addition of different concentrations of extract.

The corrosion rate of Cu metal was determined by two different techniques using the same instrument, EIS and EFM techniques. EIS and EFM calculations were determined by Gamry's framework and Echem analyst software. Plotting, graphing, and fitting data take place by Gamry software application. A frequency range of 100 kHz to 10 mHz with amplitude of 5 mv peak using AC signals was used to determine EIS parameters. Two frequencies 2 and 5 Hz were used in EFM experiments. Three evidences were used for selection between 2 and 5 Hz. Corrosion current densities, Tafel slopes and causality factors were calculated using larger peaks.

## 2.5. Surface Analysis

Cu pieces are soaked in several test solutions for a full day, isolated and dried. The shape of the surface of metal pieces was investigated by AFM technique. The composition of the corrosion product formed on the Cu surface was examined by FT-IR spectroscopic study

### 2.5.1 AFM technique

Roughness data from different surfaces is measured by AFM which act as a powerful technique. AFM is becoming an accepted technique of roughness investigation [49,50]. AFM provided that direct insight into the changes in the surface shape take places at several hundred nanometers when topographical changes due to the initiation of corrosion and formation of caring film on the metal in the presence of inhibitors. AFM device model is a Pico SPM2100. Three and two dimension images were obtained from AFM device operating in contact mode in air at nanotechnology Laboratory, Faculty of Engineering Mansoura University. AFM images were scanned at a  $5 \mu\text{m} \times 5 \mu\text{m}$  areas at a scan rate of 2.4 lines per second.

### 2.5.2 FT-IR Spectra

IR Affinity (Perkin-Elmer) spectrophotometer was used for recording the FT-IR spectra of the up late and lupine extract (crude) at central laboratory in Faculty of Pharmacy, Mansoura University. A frequency range of the device is adjusted to the range between  $4000\text{-}400 \text{ cm}^{-1}$ .

## 3. RESULT AND DISCUSSION

### 3.1. WL method

Calculated data show that, by increasing concentration of the extract, surface coverage ( $\Theta$ ) and hence %IE increases, but corrosion rate (C.R) decreases. WL-time curves of Cu in 2 M  $\text{HNO}_3$  acid solution studied in the temperature  $25^\circ\text{C}$  shown in Fig. (1)

**Table 1.** Variation of  $\Theta$  and %IE of lupine seed extract at 120 min immersion in 2 M  $\text{HNO}_3$  at  $25^\circ\text{C}$

[inh] Ppm	C.R $\times 10^{-3}$ ( $\text{mg cm}^{-2}\text{min}^{-1}$ )	$\Theta$	% IE
50	44	0.166	16.64
100	23	0.561	56.11
150	22	0.582	58.2
200	18	0.654	65.4
250	17	0.681	68.1

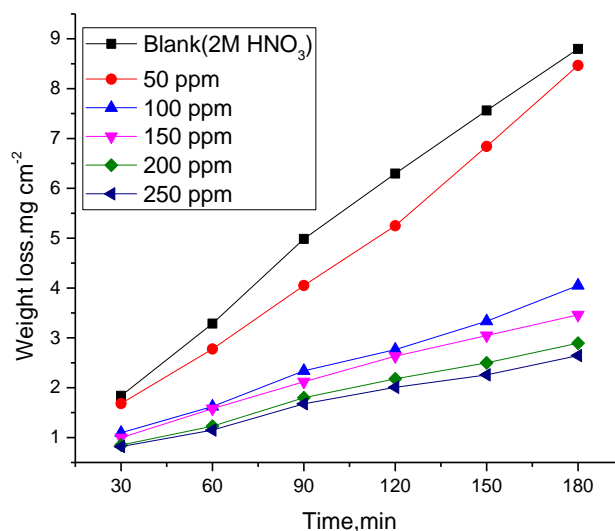


**Figure 1.** WL-time scheme for the corrosion of Cu in 2 M HNO<sub>3</sub> alone and with addition of different doses of lupine seed extract at 25°C

### 3.2. Action of BaCl<sub>2</sub> on the IE of Lupine Seed Extract

The action of BaCl<sub>2</sub> on the inhibition efficiency of Lupine is given in Table 2. It is observed that a given concentration of BaCl<sub>2</sub> the IE increases as the concentration of Lupine increases. It is also seen that a synergistic action exists between BaCl<sub>2</sub> and Lupine. Their combination has high IE 95 percent. The synergistic action of these ion is responsibility of the strong chemisorption leads to superior surface coverage and, therefore, larger inhibition.

**Table 2.** The %IE obtained from WL method of Cu dissolution in 2 M HNO<sub>3</sub> solution at several doses of the lupine seed extract with addition of 10<sup>-3</sup> M BaCl<sub>2</sub> after 120 min. immersion at 25°C

[Inh]Ppm	Θ	% IE
50	0.954	92.42
100	0.968	93.42
150	0.967	94.82
200	0.970	95.01
250	0.973	95.21

A parameter S<sub>θ</sub> was used to correct the synergistic inhibition action. The surface coverage values (θ) of the anion, cation and both were used to calculate S<sub>θ</sub>. The synergism parameter S<sub>θ</sub> can be considered by Aramaki and Hackerman using the mathematical equation (3) [51]:

$$S_{\theta} = 1 - \theta_{1+2} / 1 - \theta'_{1+2} \tag{3}$$

Where:  $\theta_{1+2} = (\theta_1 + \theta_2) - (\theta_1\theta_2)$ ;  $\theta_1$  = surface encasement via BaCl<sub>2</sub>;  $\theta_2$  = surface encasement via lupine extract;  $\theta'_{1+2}$  = measured surface encasement via BaCl<sub>2</sub> and lupine together.

### 3.2.1 Synergism parameter

The value of synergism parameter is shown in Table 3, here values of  $S_{\theta}$  are greater than 1 telling a synergistic effect.  $S_{\theta}$  approaches 1 when no interaction occurs between the inhibitor's compounds. If  $S_{\theta} > 1$  it shows that the synergistic action happens between the inhibitor's compounds. In the case of  $S_{\theta} < 1$  the negative interaction of inhibitor succeeds (i.e. the corrosion rate increases). Table 3 indicates that the values of synergism parameters ( $S_{\theta}$ ) calculated from surface are greater than one.

Based on that, a synergistic effect exists between  $\text{BaCl}_2$  and Lupine [52-54]. Thus, the enhancement of the inhibition efficiency caused by the addition of Lupine to  $\text{BaCl}_2$  is due to the synergistic effect.

**Table 3.** IE and  $S_{\theta}$  for various doses of Lupine seed extract- $\text{BaCl}_2$ , when Cu immersed in 2M  $\text{HNO}_3$ .

$\text{BaCl}_2$ M	Inhibition Efficacy IE (%)	Surface Coverage $\Theta_1$	Lupine Extract ppm	Inhibition Efficiency IE (%)	Surface Coverage $\Theta_2$	Combined IE %	Combined Surface Coverage $\theta'_{1+2}$	Synergism parameter $S_{\theta}$
$10^{-3}$	45.1	0.451	50	16.6	0.166	92.4	0.924	5.8
$10^{-3}$	45.1	0.451	100	56.1	0.561	93.4	0.934	3.5
$10^{-3}$	45.1	0.451	150	58.2	0.582	94.8	0.948	3.9
$10^{-3}$	45.1	0.451	200	65.4	0.654	95.0	0.950	3.9
$10^{-3}$	45.1	0.451	250	68.1	0.681	95.2	0.952	3.5

### 3.3. PP measurements

Cathodic and anodic polarization curves resulting from copper in nitric acid alone and copper in acid with addition of different concentrations of inhibitor are used to determine the current potential characteristics which shown in Fig. 2. Corrosion current ( $i_{\text{corr}}$ ), corrosion potential ( $E_{\text{corr}}$ ) and cathodic Tafel ( $\beta_c$ ) are determined from both lupine extract and  $\text{BaCl}_2$  at different concentrations in 2M of acid. These results are shown in table 4. The inhibition efficiency can be determined in case of polarization according to the mathematical equation (4):

$$\text{IE\%} = (1 - i_{\text{corr}} / i_{\text{corr}}^{\circ}) \times 100 \quad (4)$$

Where  $i_{\text{corr}}^{\circ}$  is the corrosion current density for Cu in acid alone and  $i_{\text{corr}}$  is the corrosion current density for Cu in acid with addition of different concentrations of inhibitor, where the plot can be determined by extrapolation of cathodic Tafel lines to corrosion potential.

**Table 4.** Effect of inhibitor concentrations on the free corrosion potential ( $E_{corr}$ ), corrosion current density ( $i_{corr}$ ), Tafel slopes ( $\beta_c$ ,  $\beta_a$ ), corrosion rate ( $k_{corr}$ ), grade of surface coverage ( $\theta$ ), and inhibition effectiveness (%IE) of Cu in 2 M of nitric acid solution at 25 °C

[Inh.] ppm	$-E_{corr}$ , mV vs SCE	$i_{corr}$ $\mu\text{A cm}^{-2}$	$\beta_c$ mV dec <sup>-1</sup>	$\beta_a$ mV dec <sup>-1</sup>	$k_{corr}$ mmy <sup>-1</sup>	$\theta$	%IE
Blank	589	301	248.6	66.1	148.3	-----	-----
50	359	117	143.8	110.0	56.38	0.612	61.2
100	568	111	71.3	241.3	53.45	0.631	63.1
150	493	82.8	75.8	208.3	40.02	0.725	72.5
200	471	69.4	79.8	173	33.55	0.769	76.9
250	59.2	30.5	269.8	107.3	15.03	0.899	89.9

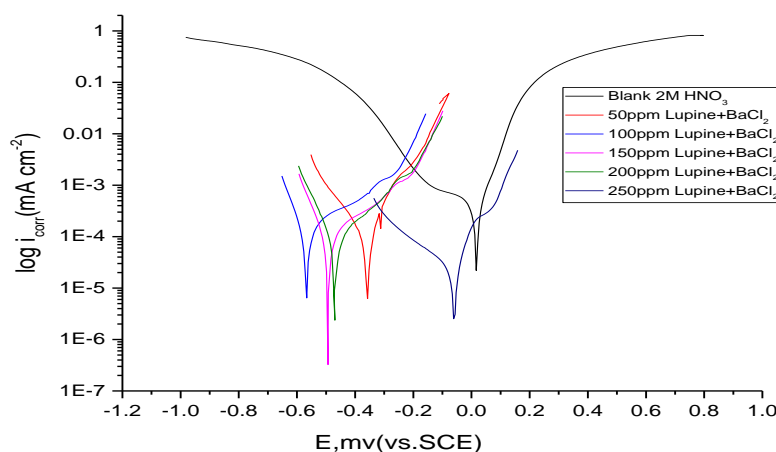


**Figure 2.** Tafel polarization scheme for Cu in 2M HNO<sub>3</sub> for several doses of Lupine seed extract + 10<sup>-3</sup> M BaCl<sub>2</sub>

Figure 2 and Table 4 indicate that there was a significant increase in parallel Tafel lines which indicates that the cathodic reaction is under controlled. Generally, the dose of extract is inversely proportional to the cathodic current density even though, there was a slight effect is detected on the anodic portions. This result showed that the inhibition increases as a result of the adsorption of the extract on the cathodic sites of the copper surface. The IE increases to reach 89.9 % with extract dose 10<sup>-3</sup> M of BaCl<sub>2</sub> + 250 ppm of lupine seed extract which indicates that cathodic reaction is significantly inhibited. The corrosion potential values deviated in no definite direction because of presence of the extract, consequences these results prove that lupine seed extract and barium chloride act as mixed type inhibitors but more cathodic.

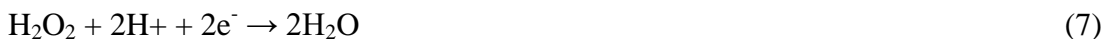
According to the well-known Pourbaix plot for Cu-water system there is no oxide film is formed to protect against the stimulation of corrosion process in the surface of the metal, where the oxygen is dissolved and reduced on the surface of metal, consequently the Cu is corroded in HNO<sub>3</sub> solution to the cuprous (Cu<sup>+</sup>) form [55-57].

This study ignores the hydrogen evolution reaction and focuses on the studying oxygen reduction only in the nitric acid solutions at potentials adjacent to the corrosion potential [58]. Studies

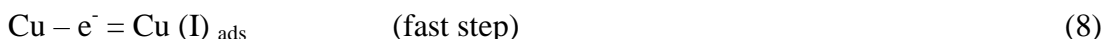
showed that there are two different mechanisms which control the cathodic reduction of oxygen which is showed in Eq. where  $4e^-$  are transferred.



The second mechanism includes two consecutive  $2e^-$  steps which involve a reduction to hydrogen peroxide first, Eq.6, followed by a further reduction, according to Eq. 7 [59]:



Oxygen reduction occurs difficulty because of the rate of oxygen reduction influenced by the transfer of oxygen from the bulk solution to the Cu solution interface, two mechanisms occurred and include  $4e^-$  transfer or two consecutive  $2e^-$  transfer. Dissolution mechanism of Cu in  $HNO_3$  occurs according to the following equations:



From the previous equation, it was found that  $Cu(I)_{ads}$  adsorbs at the Cu surface and does not diffuse into the bulk solution [60,61]. The diffusion of soluble Cu (II) species from the external Helmholtz plane to the bulk solution is used to prove the dissolution of Cu in acid.

Previously, it was found that the slopes of the anodic ( $\beta_a$ ) and cathodic ( $\beta_c$ ) Tafel lines continue almost unchanged and this leads to an approximately parallel set of anodic lines, and an almost parallel cathodic plot result too. This occurs as a result of addition of inhibitor under study (both lupine extract and barium chloride). Thus, the active sites for both anodic and cathodic processes are blocked by the adsorbed inhibitor. In another meaning, the surface area for corrosion is decreased by the adsorbed inhibitor and this is occurring without touching the corrosion mechanism of Cu in these solutions, and preventing a part of the surface with respect to the destructive medium [62,63].

### 3.4. EIS measurements

The corrosion actions of Cu in 2M  $HNO_3$  solution in the absence and presence of different concentrations of Lupine extract +  $BaCl_2$  was investigated by the EIS technique at  $25 \pm 1^\circ C$ . Figures (3-4) show the Nyquist and Bode schemes for Cu in 2 M  $HNO_3$  solution in the absence and presence of different concentrations of aqueous extract and  $BaCl_2$  compounds at  $25^\circ C$ . The frequency dispersion resulting from irregularity of the electrode surface leads to make the Nyquist impedance plot is not perfect semicircle in some cases [64]. Previous studies have shown that, the impedance graph consists of low frequencies dispersion with large capacitive loop. These low frequencies dispersion (inductive arc) are referred to anodic adsorbed intermediates dominant the anodic progression [65, 66]. Consequence this, the low frequency dispersion was ignored.

The experimental data of the different impedance graph the Nyquist (a) and Bode (b) plots Figs. (3, 4) were determined by fitting it to a simple equivalent circuit model as shown in Figure. (5), which includes the double layer capacitance  $C_{dl}$  and solution resistance  $R_s$  which is set in parallel to the charge transfer resistance  $R_{ct}$  [67].

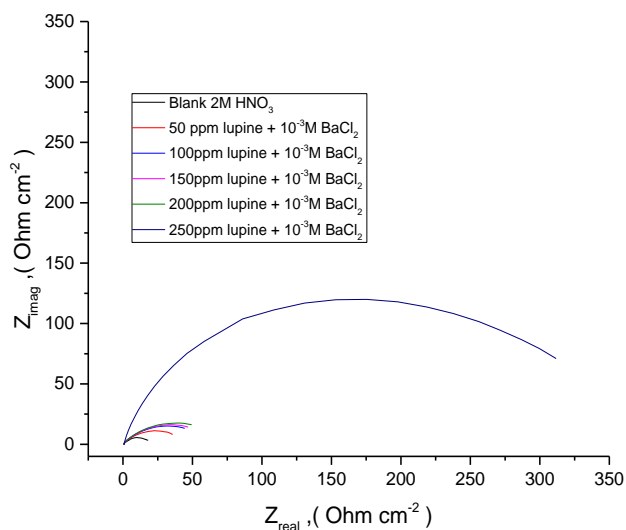


**Figure 3.** The Nyquist graphs for the corrosion of Cu in 2M HNO<sub>3</sub> alone and in the existence of different doses of Lupine seed extract and 10<sup>-3</sup> M BaCl<sub>2</sub> at 25°C

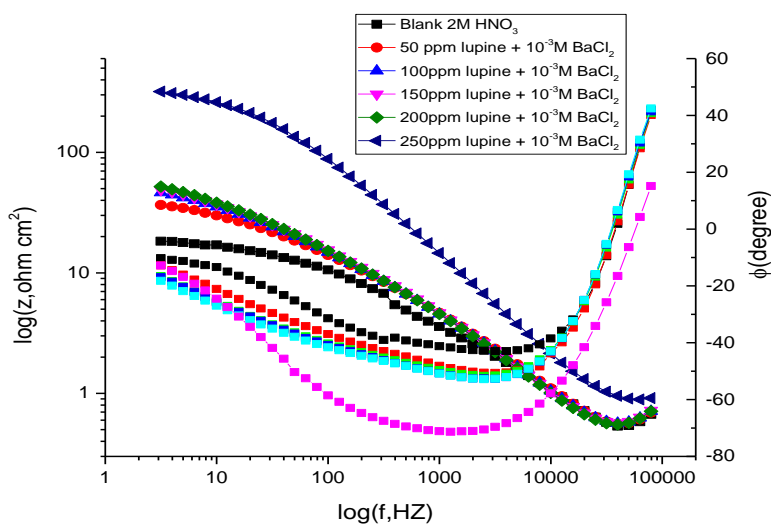


**Figure 4.** Bode graphs for the corrosion of Cu in 2 M HNO<sub>3</sub> alone and in the existence of different doses of Lupine seed extract and 10<sup>-3</sup> M BaCl<sub>2</sub> at 25°C

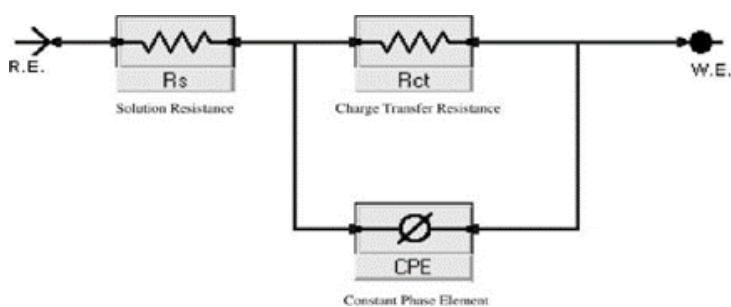


**Figure 5.** Electrical equivalent circuit model used to fit the results of impedance

**Table 5.** EIS parameters for the corrosion of Cu in 2 M HNO<sub>3</sub> alone and in the existence of several doses of Lupine seed extract and 10<sup>-3</sup> M BaCl<sub>2</sub> at 25°C

Conc. ppm	C <sub>dl</sub> μF cm <sup>-2</sup>	R <sub>ct</sub> Ω cm <sup>2</sup>	α	Y <sub>0</sub> x10 <sup>-4</sup> μΩ <sup>-1</sup> sn m <sup>-2</sup>	θ	% IE
Blank	11.2	19.74	0.69	7.2	---	-----
50	7.5	37.66	0.71	5.6	0.476	47.6
100	4.87	51.69	0.69	6.3	0.618	61.8
150	4.76	53.88	0.71	6.2	0.634	63.4
200	4.18	60.44	0.69	6.3	0.673	67.3
250	0.67	329.5	0.87	7.2	0.940	94.0

A single semi-circle moved along the real impedance ( $Z_r$ ) axis as shown in this graph. The increase of concentrations leads to display single capacitive loop in the graph, as a result of charge transfer of the corrosion process, and therefore the diameters of the loops increase. EIS information shown that as the concentration of inhibitor increase  $R_{ct}$  increase and  $C_{dl}$  decrease. Also, it was found that the inhibition efficiency increase when  $R_{ct}$  values increase. This increase in IE% because of the gradual replacement of water molecules by the adsorption of the inhibitor molecules on the metal surface. This indicates to form a supporter film on the metal surface, and this explains that the coverage of the metal surface resulting from film decreases the double layer thickness. Also, the increase of inhibitor concentration leads to decrease the double layer thickness at the metal/solution interface. This decrease of  $C_{dl}$  produced from a decrease in local dielectric constant. Previously, it was found that the inhibitors were adsorbed on the surface at both anodic and cathodic spots [68]. The experimental data of Nyquist graphs can be determined by using the circuit in Fig. (5), in which,  $R_{ct}$  represents the charge-transfer resistance,  $R_s$  represents the electrolyte resistance and the constant phase element (CPE). The inhibition behavior of the inhibitor resulting from other procedures was confirmed by the impedance data.

### 3.5. EFM measurements

The corrosion current values can be determined quickly and directly by a nondestructive EFM procedure and this can be done with only a small polarizing signal and without prior knowledge of Tafel slopes. These advantages of EFM procedure make it an ideal applicant for online corrosion monitoring [69]. EFM is the great technique because of presence of the causality factors which attend as an internal check on the validity of the EFM quantity. Quality control can be applied on the experimental EFM data by the causality factors. It has been shown in Fig (6) that the current response contains frequency components which are the difference, sum, and multiples of the two input frequencies. The corrosion current density ( $i_{corr}$ ), the Tafel slopes ( $\beta_a$  and  $\beta_c$ ) and the causality factors (CF-2 and CF-3) were determined by using the larger peaks. These parameters at several concentrations of inhibitor in acidic solution at 25°C were recorded in Table (6). The % IE can be

calculated from mathematical equation (10). It was observed that% IE increases by increasing the extract doses

$$\% IE_{EFM} = [1 - (i_{corr} / i_{corr}^{\circ})] \times 100 \tag{10}$$

Where  $i_{corr}^{\circ}$  is the corrosion current density for Cu in acid alone and  $i_{corr}$  is the corrosion current density for Cu in acid with addition of different doses of extract. The obtained data are in good quality as a result of the measured causality factors CF-2 and CF-3 in Table (6) are near to their theoretical values of 2.0 and 3.0, respectively. The calculated IE which obtained from other methods WL, PP and EIS measurements compatible with the results that obtained from EFM measurements.

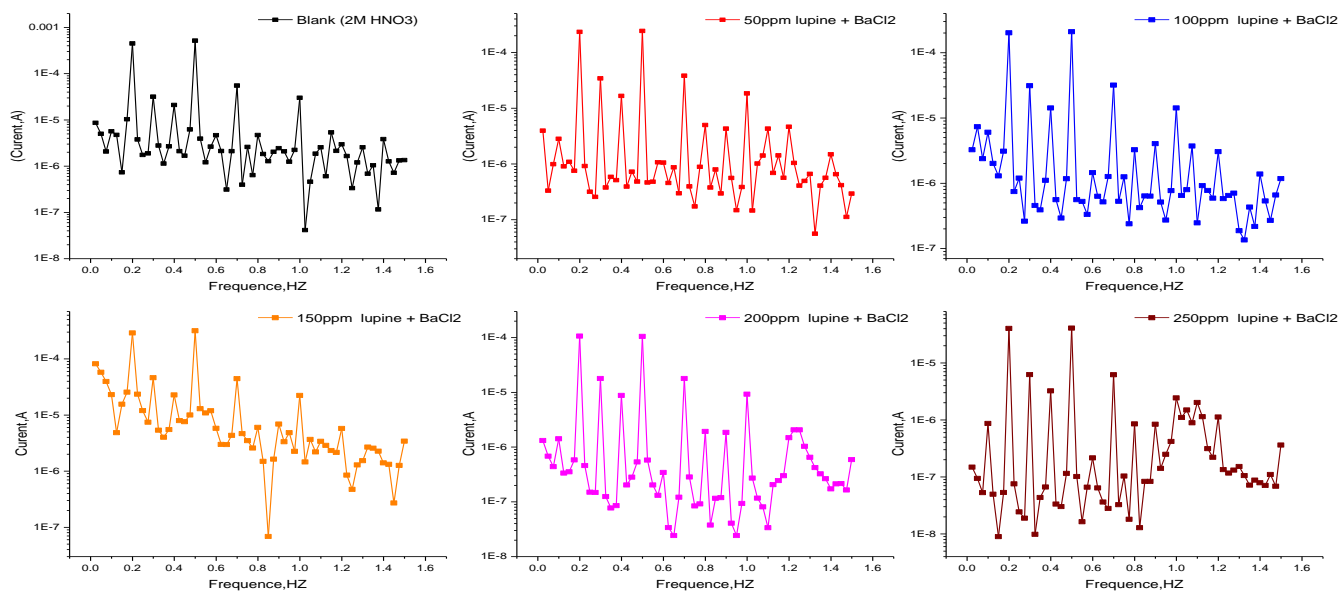


**Figure 6.** EFM spectra for Cu in 2 M HNO<sub>3</sub> alone and in the existence of different doses of Lupine seed extract + 10<sup>-3</sup>M BaCl<sub>2</sub>

**Table 6.** Parameters obtained by EFM performance for Cu in nitric acid HNO<sub>3</sub> in the absence and presence of several doses of Lupine seed extract + 10<sup>-3</sup>M BaCl<sub>2</sub> in 2 M HNO<sub>3</sub> at 25°C

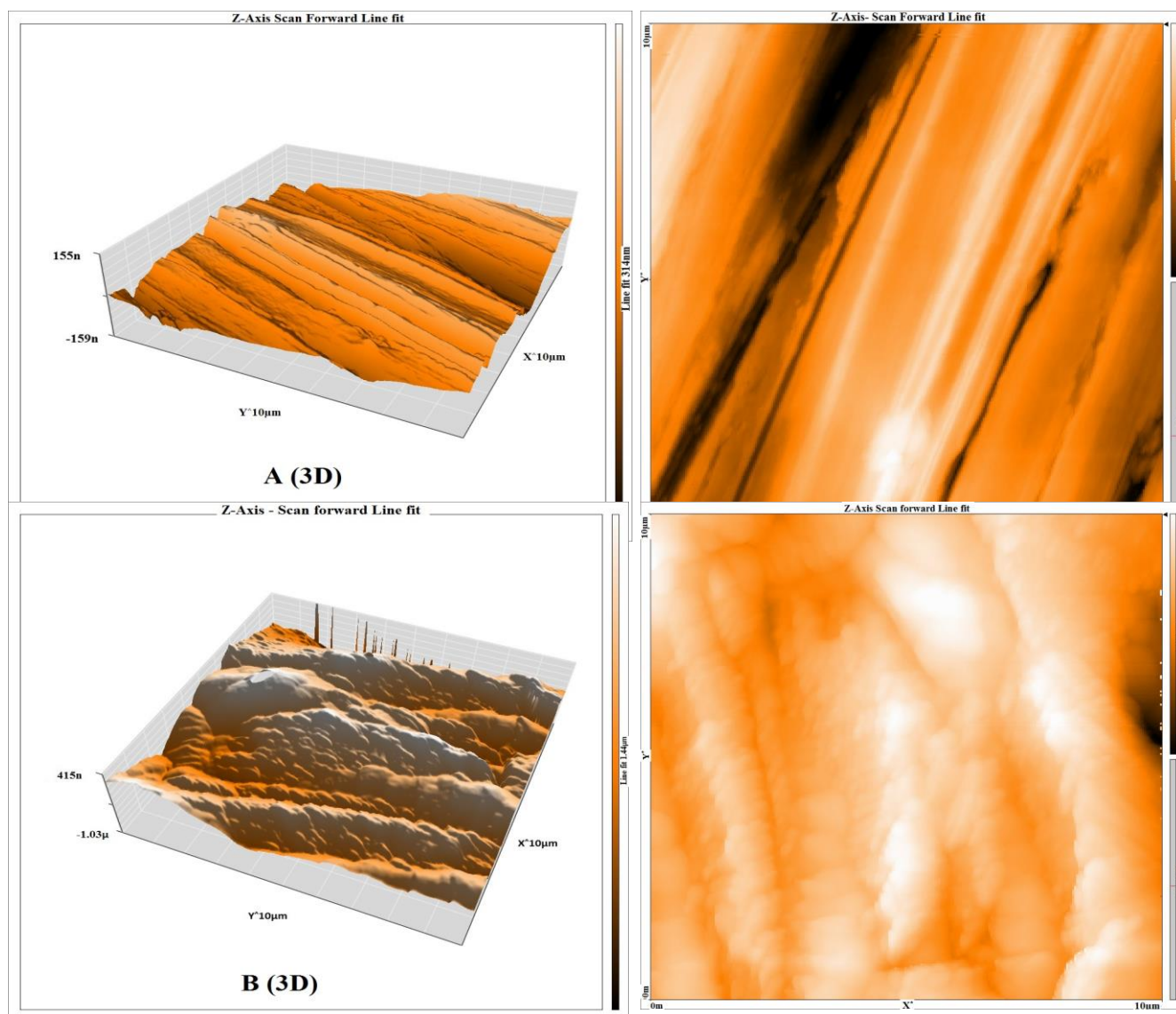
Conc., ppm	$i_{corr}$ $\mu A\ cm^{-2}$	$\beta_c$ $mVdec^{-1}$	$\beta_a$ $mVdec^{-1}$	CF-2	CF-3	$\theta$	$IE_{EFM}\%$
0	1186	289	111	1.7	3.53	---	---
50	447.4	287	78	2.07	3.19	0.623	62.3
100	344.5	225	72	2.21	3.11	0.709	70.9
150	331.9	106	54	2.00	2.3	0.720	72.0
200	260.5	901	88	1.98	3.56	0.780	78.0
250	60.71	181	67	2.19	3.19	0.949	94.9

### 3.6. Atomic Force microscopy (AFM)

AFM is a very important technique for measuring the roughness of a sample surface at a high resolution in the order of fraction of nanometer [70]. AFM measurements are able to give details about the surface morphology of copper metal which is useful to corrosion science research. The three dimensional (3D) and two dimensional (2D) of AFM images appear as shown in Fig.7. Cu metal before immersion appear in Fig. 7a, Cu immersed in 2 M HNO<sub>3</sub> for 24 hours appear in Fig 7b and Cu immersed in acid with addition of lupine seed extract (250 ppm) and barium chloride (10<sup>-3</sup>M) in Fig.7c for 24 hours.

#### 3.6.1 Root Mean square roughness and average roughness

The average roughness R<sub>a</sub> can be defined as the average deviation of all points roughness profile that are measured from a mean line. Also, Root mean square roughness, R<sub>q</sub> is the average deviation that are measured from the mean line.



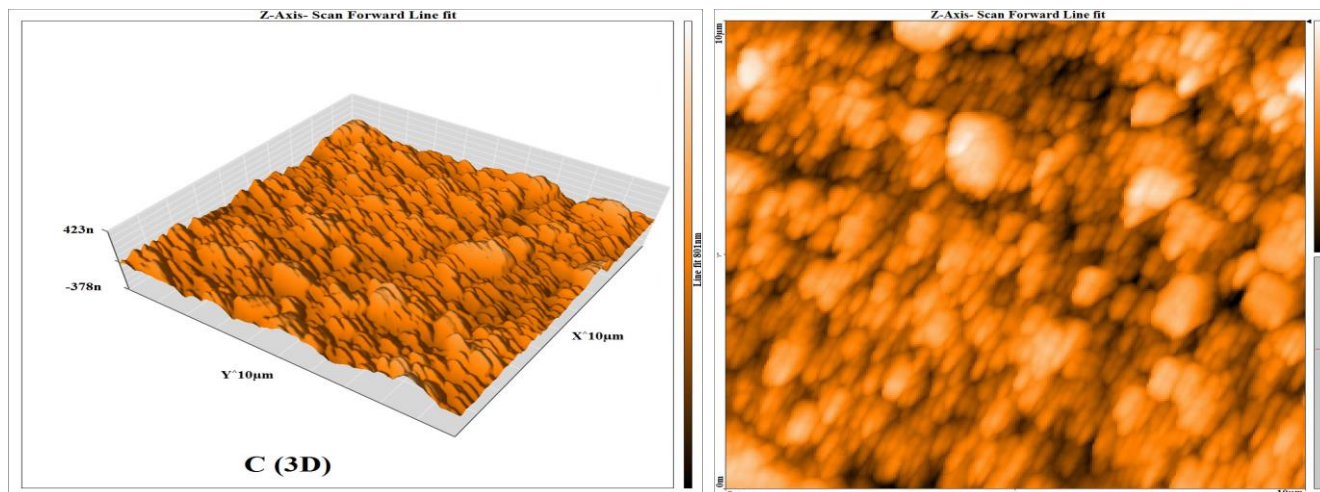


**Figure 7.** The two-dimensional (2D) and three-dimensional (3D) AFM images (A) Cu metal before immersion in acid (reference) (B) Cu metal immersed in 2M HNO<sub>3</sub> alone (blank) (C) Cu metal immersed in 2M HNO<sub>3</sub> with addition of Lupine seed extract (250 ppm) + BaCl<sub>2</sub>(10<sup>-3</sup>M)

The average roughness and root mean square roughness can be measured from AFM image. R<sub>q</sub> is much more sensitive than R<sub>a</sub> to large and small high deviations from the mean [71]. Table (8) gives the corresponding average roughness R<sub>a</sub> and RMS roughness (R<sub>q</sub>) values. A proportional view of the above roughness table clearly establishes that the surface of the metal is smoothed due to the adsorption coating formed [72]

**Table 8.** AFM roughness data

Specimen	Average roughness(R <sub>a</sub> ) nm	RMS roughness (R <sub>q</sub> ) nm
Polished u metal surface (reference)	24.87	31.62
Cu metal immersed in 2M HNO <sub>3</sub> (blank)	163.06	203.14
Cu metal immersed in 2M HNO <sub>3</sub> containing Lupine extract (250 ppm) + BaCl <sub>2</sub> (10 <sup>-3</sup> M)	36.19	45.33

### 3.7. FT-IR spectral analysis

Figure 8a, b represents the IR spectrum of lupine extract (crude) and that of the film created on the Cu immersed in 2M HNO<sub>3</sub>, lupine (250ppm) and BaCl<sub>2</sub> (10<sup>-3</sup>M). The FTIR spectrum of pure Lupine extract appears in Fig 8a. The -OH stretching frequency at 3419 cm<sup>-1</sup>, the -CH stretching frequency at 2933 cm<sup>-1</sup>, the C=O stretching frequency appears at 1654 cm<sup>-1</sup>, the -C=C stretching frequency appears at (1405-1547 cm<sup>-1</sup>) (multiple bands), the -CN stretching frequency appears at 1246, 2923 cm<sup>-1</sup>. The C=O stretching frequency shifts from 1654 cm<sup>-1</sup> to 1681 cm<sup>-1</sup>. The -C=C stretching frequency shifts from 1405 cm<sup>-1</sup> to 1417 cm<sup>-1</sup>. The -CN stretching frequency shifts from 1246 cm<sup>-1</sup> to 1294 cm<sup>-1</sup>. The -CO stretching frequency shifts from 1055 cm<sup>-1</sup> to 1045 cm<sup>-1</sup>. Cu-O Vibrations leads to

the absorption peaks in the infrared spectrum at low frequencies below  $700\text{ cm}^{-1}$ . [73] Similar results for the structure of copper film were obtained by Armstrong and Hall [74].

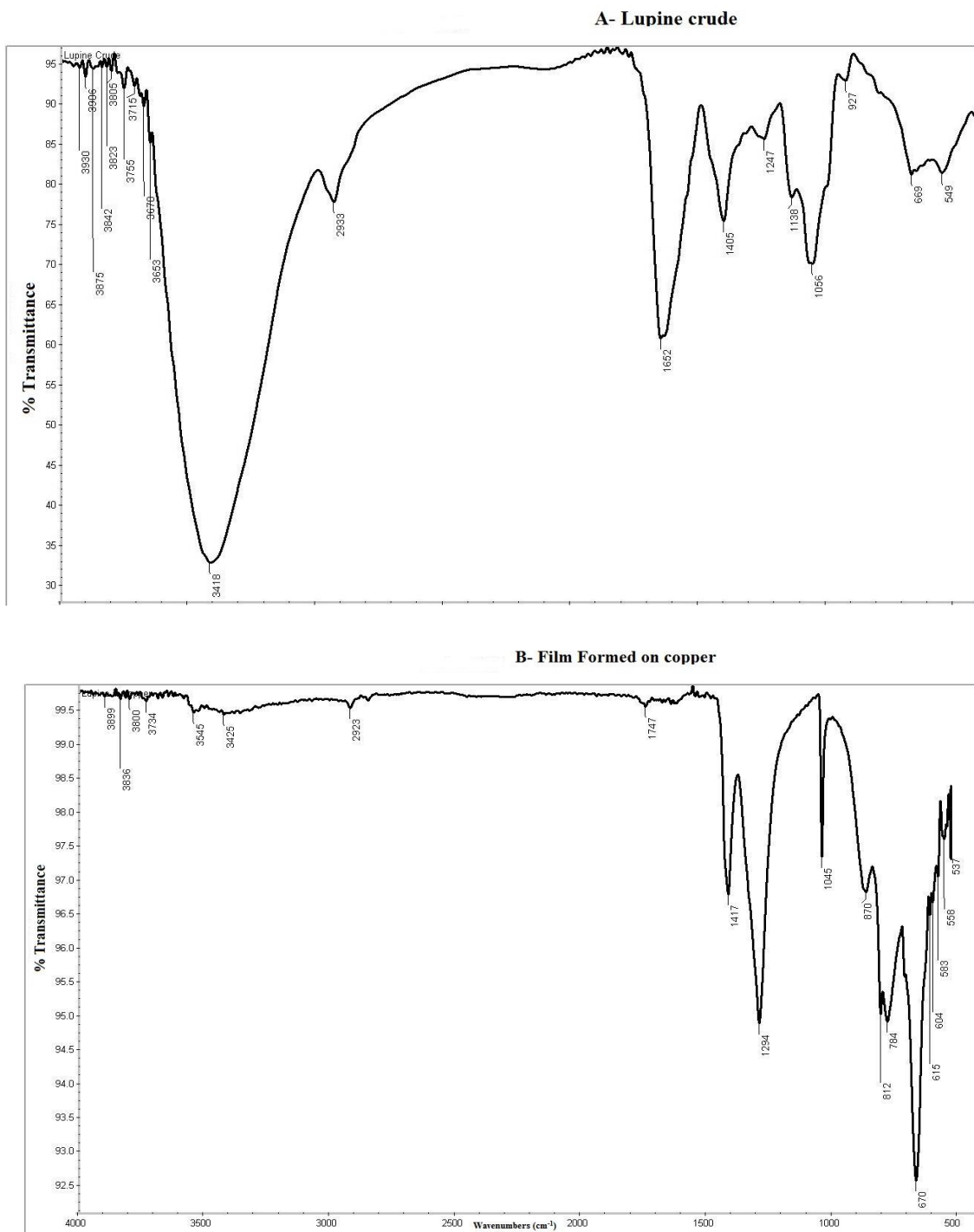
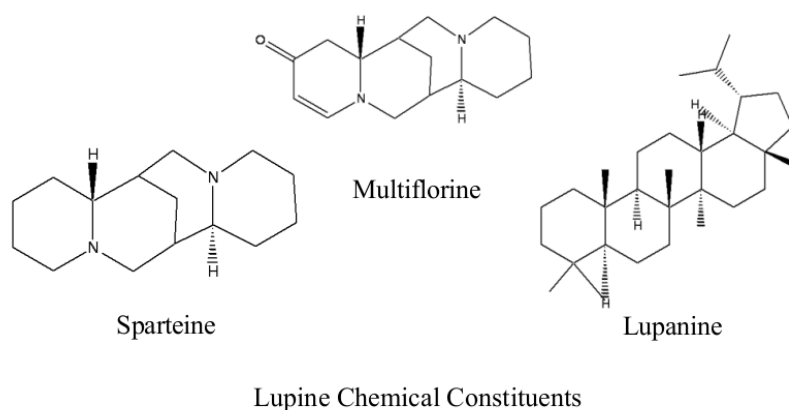


**Figure 8.** FTIR spectra of copper in nitric acid containing optimum concentration of (a) the extract only and (b) The extract on copper surface

The FTIR spectrum of the film formed on the copper immersed in 2 M  $\text{HNO}_3$ , lupine (250 ppm) and  $\text{BaCl}_2$  ( $10^{-3}\text{M}$ ) appears in Fig 8b. The  $-\text{CH}$  stretching frequency shifts from  $2933\text{ cm}^{-1}$  to  $\text{cm}^{-1}$  and the  $-\text{CO}$  stretching frequency appears at  $1055\text{ cm}^{-1}$ .

### 3.8. Mechanism of corrosion inhibition

The plant extracts are organic in nature, containing the bioactive compounds which are effective like synthetic inhibitors. These bioactive compounds act as inhibitors in acid solution which interact with metals and affect the corrosion reaction in a number of ways. The chemical composition of the aqueous extract seeds of lupine (*Lupinus termis* L) indicates the existence of 50% protein, 20% lipids and 5% quinolizidine alkaloids. Investigation of the alkaloid content describe that the quinolizidine lupine alkaloids especially lupanine were the most abundant; multiflorine was also present. Moreover, the sparteine found in the lupine extract act as a dibasic quinolizidine alkaloid [47]. It is therefore appropriate to say that the adsorption of these compounds onto metal surface is responsible for corrosion inhibition effect and hence difficult to assign the inhibitive effect to a particular constituent.



## 4. CONCLUSIONS

The extract of lupine seed inhibits the Cu corrosion in  $\text{HNO}_3$  medium. Addition of barium chloride to the extract showed synergistic action on the corrosion inhibition efficiency towards Cu in acidic medium. The extract functions as it is shown by the polarization studies are a mixed inhibitor. The inhibition efficiency obtained from different tests, WL, PP, EIS and EFM and EFM measurements converging with each other. The existence of the protective film on the surface of Cu was proved by AFM analysis and FT-IR spectra.

## References

1. V. Oteino-Alergo, N. Huynh, T. Notoya, S. E. Bottle, D. P. Schwcinsberg, *Corros. Sci.*, 41 (1999) 685.
2. H. Y. Tsai, S. C. Sun, S. J. Wang, *J. Electrochem. Soc.*, 147 (2000) 2766.
3. A. Krishnamoorthy, K. Chanda, S. P. Murarka, G. Ramanath, J. G. Ryan, *Appl Phys Lett.*, 78 (2001) 2467.
4. C. E. Ho, W. T. Chen, C. R. Kao, *J Electron Mater*, 30 (2001) 379.
5. U. R. Evans, *Trans Farad Soc.*, 40 (1944) 120.
6. A. I. Krosilshchikov, I. V. Dedova, *J Gen Chem U.S.S.R.*, 16 (1946) 537.

7. Y. Komuro, *J Chem Soc Jpn.*, 75 (1954)255.
8. E. A. Travincek, J. H. Weber, *J Phys Chem.*, 65 (1961) 235.
9. I. S. Smol'yaninov, I. Voronezhsk, *Gos Ped Inst.*, 47 (1964)34.
10. A. Rasheed Arain, A. M. Shams El Din, *Thermochim Acta*, 89 (1985) 171.
11. A. Zarrouk, A. Dafali, B. Hammouti, H. Zarrok, S. Boukhris, M. Zertoubi, *Int. J. Electrochem. Sci.*, 5 (2010) 46.
12. A. Zarrouk, T. Chelfi, A. Dafali, B. Hammouti, S.S. Al-Deyab, I. Warad, N. Benchat, M. Zertoubi, *Int. J. Electrochem. Sci.*, 5 (2010) 696.
13. A. Zarrouk, I. Warad, B. Hammouti, A. Dafali, S.S. Al-Deyab, N. Benchat, *Int. J. Electrochem. Sci.*, 5 (2010) 1516.
14. A. Zarrouk, B. Hammouti, A. Dafali, H. Zarrok, *Der Pharma Chemica.*, 3 (2011) 266.
15. A.S. Fouda, H. A. Wahed, *Arab. J. Chem.*, 9 (2016) S91.
16. A.S. Fouda, M. M. Gouda and S. I. Abd El-Rahman, *Bull. Korean Chem. Soc.*, 21 (2000) 1085.
17. K. F. Khaled, Mohammed A. Amin, *Corros. Sci.*, 51 (2009) 2098.
18. K. F. Khaled, Sahar A. Fadl-Allah, B. Hammouti, *Mater. Chem. Phys.*, 117 (2009) 148.
19. M. Mihit, K. Laarej, H. Abou El Makarim, L. Bazzi, R. alghi, B. Hammouti, *Arab. J. Chem.* 3 (2010) 55.
20. A. Fiala, A. Chibani, A. Darchen, A. Boulkamh, K. Djebbar, *Appl. Surf. Sci.*, 253 (2007) 9347.
21. A. Howida, Fetouh, M. Tarek and Abdel-Fattah, *Int. J. Electrochem. Sci.*, 9 (2014) 1565.
22. K. T. Knecht, H. Nguyen, A. D. Auke, D. H. Kinder, *J Herb Pharmacother.*, 6 (2006) 89.
23. M. Abdel-Gaber, B. A. Abd-El-Nabey, I. M. Sidahmed, A. M. El-Zayady, M. Saadawy, *Corros. Sci.*, 48 (2006) 2765.
24. Emsley, John, *Nature's building blocks: An A-Z guide to the elements*, Oxford University Press, (2003) 121.
25. Günter Joseph, J. A Konrad Kunding, *ASM International*, (1999) 348.
26. E. M. Mannebach et al., *Andrew Gordon*, 650 (2015) 926.
27. L. Valek, S. Martinez, *Mater. Lett.*, 61(1) (2007) 148.
28. A.M. Shah, A.A. Rahim, S.A. Hamid, S. Yahya, *Int. J. Electrochem. Sci.*, 8 (2013) 2140.
29. B.A. Abd-El-Nabey, A.M. Abdel-Gaber, M.E.S. Ali, Khamis E, S. El-Housseiny, *Int. J. Electrochem. Sci.*, 8 (2013) 5851.
30. R. Senthoran, N. Priyantha, *Ann. Res. J. SLSAJ*, 12 (2012) 131.
31. E.A. Noor, *J. Appl. Electrochem.*, 39 (9) (2009) 1465.
32. A. Minhaj, P.A. Saini, M.A. Quraishi, I.H. Farooqi, *Corros. Preven. Control*, 46(2) (1999) 32.
33. M.A. Quraishi, A. Singh, V.K. Singh, D.K. Yadav, A.K. Singh, *Mater. Chem. Phys.*, 122(1) (2010) 114.
34. I.E. Uwah, P.C. Okafor, V.E. Ebiekpe, *Arab. J. Chem.*, 6(3) (2013) 285.
35. P.C. Okafor, E.E. Ebenso, U.J. Ekbe, *Int. J. Electrochem. Sci.*, 5(7) (2010) 978.
36. M. El-Sayed, O.Y. Mansour, I.Z. Selim, M.M. Ibrahim, *J. Sci. Ind. Res.*, 60(9) (2001) 738.
37. J.C. da Rocha, J.A. da Cunha Ponciano Gomes, E. D'Elia, *Corros. Sci.*, 52(7) (2010) 2341.
38. P.C. Okafor, M.E. Ikpi, I.E. Uwah, E.E. Ebenso, U.J. Ekpe, S.A. Umoren, *Corros. Sci.*, 50(8) (2008) 2310.
39. P.C. Okafor, E.E. Ebenso, *Pigm. Resin Technol.*, 36(3) (2007) 13440.
40. C.A. Loto, *Corros. Prev. Control*, 48(2) (2001) 59.
41. C.A. Loto, *Corros. Prev. Control*, 48(1) (2001) 38.
42. I.B. Obot, N.O. Obi-Egbedi, *Int. J. Electrochem. Sci.*, 4(9) (2009) 1277.
43. S.A. Umoren, I.B. Obot, E.E. Ebenso, N.O. Obi-Egbedi, *The Desalination*, 247(1–3) (2009) 561.
44. Xianghong Li, Shuduan Deng, *Corros. Sci.*, 65 (2012) 299.
45. E.E. Oguzie, *Corros. Sci.*, 49(3) (2007) 152746.
46. P.B. Raja, M.G. Sethuraman, *Mater. Lett.*, 62(17–18) (2008) 2977.
47. B. A. Abd-El-Naby, O. A. Abdullatef, A. M. Abd-El-Gabr, *Int. J. Electrochem. Sci.*, 7 (2012) 5864.

48. A. J. Abdul Nasser, V. Rethina Giri, S. Karthikeyan, K. N. Srinivasan, *Der Chemica Sinica*, 3(2) (2012) 402.
49. Z. Khiati, A.A. Othman, M. Sanchez-Moreno, M. C. Bernard, S. Joiret, E.M.M Sutter, V. Vivier, *Corros. Sci.*, 53 (2011) 3092.
50. Benita Sherine, A. Jamal Abdul Nasser, S. Rajendran, *Inter. J. Eng. Sci. Techol.*, 2(4) (2010) 341.
51. K. Aramaki, and N. Hackerman, *J. Electrochem. Soc.*, 1169 (5) (1969) 568.
52. S.A.M.Refaey, F. Taha and A.M. Abd El-Malak, *Int. J. Electrochem. Sci.*, 1(2006) 80.
53. B M Mistry et al, *Bull. Mater. Sci.*, 35(3) (2012) 459.
54. M. Ebadi, W. J. Basirun, S. Y. Leng and M.R. Mahmoudian, *Int. J. Electrochem. Sci.*, 7 (2012) 8052.
55. M.A. Schumacher, and W. J. Muller, *Electroanal. Chem.*, 219 (1987) 311.
56. W.D. Bjorndahl and K. Nobe, *Corrosion*, 40 (1984) 82.
57. G. Quartarone, G. Moretti, T. Bellomi, G. Capobianco and A. Zingales, *Corrosion*, 54 (1998) 606.
58. W.H. Smyrl in: J. O'M. Bockris, B.E. Conway, E. Yeager and R.E. White, Editors, *Comprehensive Treatise of Electrochemistry, Plenum Press, New York*, 4 (1981) 116.
59. P. Jinturkar, Y.C. Guan and K.N. Han, *Corrosion*, 54 (1984) 106.
60. T. Hurlen, G. Ottesen and A, *Electrochim. Acta*, 23 (1978) 39.
61. R. Caban and T.W. Chapman, *J. Electrochem. Soc.*, 124 (1977) 1371.
62. J.W. Schlitz and K. Wippermann, *Electrochim. Acta*, 32 (1987) 823.
63. H. Ashassi-Sorkhabi, N. Ghalebsaz-Jeddi, F. Hashemzadeh, H. Jahani, *Electrochim. Acta*, 51 (2006) 3848.
64. A. Caprani, I. Epelboin, Ph. Morel, H. Takenouti, proceedings of the 4th European sym. on Corros. Inhibitors, *Ferrara, Italy* (1975) 571.
65. J. Bessone, C. Mayer, K. Tuttner, W. J. Lorenz; *Electrochim. Acta*, 28 (1983) 171.
66. I. Sekine, M. Sabongi, H. Hagiuda, T. Oshibe, M. Yuasa, T. Imahc, Y. Shibata and T. Wake, *J. Electrochem. Soc.*, 139 (1992) 3167.
67. F. Bentiss, M. Traisnel and M. Lagrenee, *Corros. Sci.*, 42 (2000) 127.
68. A. M. Eldesoky, Hala. M. Hassan, A. S. Fouda, *Int. J. Electrochem. Sci.*, 8 (2013) 10376.
69. E. Kus, F. Mansfeld, *Corros. Sci.*, 48 (2006) 965.
70. B. Wang, M. Du, J. Zang and C.J, Gao, *Corros.Sci.*, 53 (1) (2011) 353.
71. Benita Sherine, A. Jamal Abdul Nasser, S. Rajendran, *Int. J. Eng. Sci. Techol.*, 2(4) (2010) 341.
72. S. Rajendran, C. Thangavelu and G. Annamalai, *J.Chem. Pharm.l Res.*, 4 (11) (2012) 4836.
73. M.U.A. Prathap, B. Kaur and R. Srivastava, *J. Colloid Interface Sci.*, 370 (2012) 14
74. R.D. Armstrong, C.A. Hall, the corrosion of metals in contact with ester oils containing water at 60 and 150° C, *Electrochim. Acta*, 40 (1995) 1135.